Facile preparation of self-healing superhydrophobic CeO_2 surface by electrochemical processes

Katsutoshi Nakayama[a,*], Takuya Hiraga[a], Chunyu Zhu[a, b], Etsushi Tsuji[c], Yoshitaka Aoki[a, b], and Hiroki Habazaki[a, b,*]

[a] Graduate School of Chemical Sciences and Engineering, Hokkaido University, Sapporo, Hokkaido 060-8628, Japan

[b] Division of Applied Chemistry, Faculty of Engineering, Hokkaido University, Sapporo, Hokkaido 060-8628, Japan

[c] Department of Chemistry and Biotechnology, Tottori University, Tottori 680-8552, Japan

*Corresponding authors.
E-mail address; k.nakayama@cse.hokudai.ac.jp (K. Nakayama),
habazaki@eng.hokudai.ac.jp (H. Habazaki)

Highlights

・The CeO_2-coating is formed on Type 304 stainless steel by anodic deposition.

・The hydrophilic CeO_2 surface is transformed to hydrophobic during air exposure.

・Superhydrophobic CeO_2 surface is obtained on hierarchically rough substrate.

・Superhydrophobic CeO_2 surface shows self-healing property.

Abstract

Herein we report simple electrochemical processes to fabricate a self-healing superhydrophobic CeO_2 coating on Type 304 stainless steel. The CeO_2 surface anodically deposited on flat stainless steel surface is hydrophilic, although high temperature-sintered and sputter-deposited CeO_2 surface was reported to be hydrophobic. The anodically deposited hydrophilic CeO_2 surface is transformed to hydrophobic during air exposure. Specific accumulation of contaminant hydrocarbon on the CeO_2 surface is responsible for the transformation to hydrophobic state. The deposition of CeO_2 on hierarchically rough stainless steel surface produces superhydrophobic CeO_2 surface, which also shows self-healing ability; the surface changes to superhydrophilic after oxygen plasma treatment but superhydrophobic state is recovered repeatedly by air exposure. This work provides a facile method for preparing a self-healing superhydrophobic surface using practical electrochemical processes.

Keywords: CeO_2 coating; superhydrophobicity: anodic deposition; self-healing ability

1. Introduction

Superhydrophobic solid materials have attracted much attention because of several superior functional properties including self-cleaning, anti-corrosion, anti-freezing and anti-biofouling [1-4]. Many natural surfaces, including lotus leaves, water strider legs and morpho butterfly wings, are superhydrophobic [5-9]. Superhydrophobicity of these surfaces is originating from peculiar microscopic geometrical surface morphology. For example, lotus leaves consist of numbers of micrometer-size asperities covered by nano-fibrous hydrophobic wax, resulting in superhydrophobicity [5, 6]. Superhydrophobic surface is usually defined to show a static contact angle for a water droplet greater than 150^{o} and a low contact angle hysteresis (the difference between the advancing and receding contact angles) of <10°. Inspired by nature, many artificial superhydrophobic materials have been developed [9-19], since Onda et al. reported a first example of artificial superhydrophobic fractal surface in 1996 [9].

In addition to the high roughness with fractal or hierarchical surface geometry, the surface must be composed of materials with low surface energy for superhydrophobicity. Thin organic coatings, including self-assembled fluoroalkyl monolayers, have been often introduced on rough metallic or inorganic substrates. However, such superhydrophobic surfaces have low durability because of mechanical

instability of thin organic coatings and highly rough hierarchical surfaces. Improved durability of superhydrophobic surfaces is awaited for practical application.

Recently, Azimi et al. reported that rare-earth oxide (REO) surfaces show thermally stable hydrophobicity up to 1000^{o}C without any organic coating due to their unique electronic structure [20]. They demonstrated that water droplets bounce on the surface of REO films formed by magnetron sputtering on silicon wafer. Moreover, they also revealed that REOs become superhydrophobic with textured morphology. These inorganic REOs are thermally and mechanically more stable compared to organic materials, promising as a novel durable hydrophobic coating. Therefore, hydrophobic REOs are of recent interest [21-24]. Most reports preparing hydrophobic REO coatings utilized dry processes such as sputtering [21] or atomic layer deposition [24]. Electrochemical deposition process is a simple, cost-effective and more practical method for oxide coatings [25]. This process also allows us to form a uniform oxide layer on rough and even porous substrates, suitable for fabrication of hierarchically rough superhydrophobic surfaces.

In the present study, the CeO_2 coating was prepared by anodic deposition on flat and hierarchically rough stainless steel surface. The rough stainless steel surface was prepared by electrochemical etching. The surface wettability for water was evaluated by measuring static and dynamic contact angles. The CeO_2 surface immediately after deposition was hydrophilic, but transformed to hydrophobic during air exposure. The self-healing properties of the hydrophilic surface was also examined in the present study.

2. Experimental

2.1 Specimen preparation

Type 304 stainless steel plates or meshes (with 300, 500, 640 and 795 mesh) composed of 17–19 wt.% Cr, 8–11 wt.% Ni, < 2 wt.% Mn, < 1 wt.% Si and Fe balance were used as substrate in this study. Prior to electrochemical etching and anodic deposition, the plate substrate was electropolished in solution containing $HClO_4$ and ethylene glycol (1:9 v/v) at 20 V for 5 min below 283 K. Electrochemical etching of the plate was performed in solution containing 1.2 wt% HNO_3 and 3.6 wt% HCl at a constant current density of 1 A cm^{-2} for 200 s at 313 K [26]. For mesh specimens, etching was conducted at 1 A cm^{-2} for 1 min in order to prevent excess etching of specimens. Anodic deposition was carried out at a constant current density of 1 A cm^{-2} in solution containing 0.01 mol dm^{-3} $Ce(NO_3)_3$ and 0.05 mol dm^{-3} hexamethylenetetramine (pH 6.7) for 60 min at 333 K. The rather low concentration of $Ce(NO_3)_3$ was selected to form a thin coating to maintain the textured morphology developed by electrochemical etching. A two-electrode cell with a Type 304 stainless steel counter electrode was used for anodic deposition. For comparison, we also prepared a barrier-type anodic alumina film on aluminum plate (99.999% purity). Prior to anodizing, an aluminum plate was electropolished in solution containing $HClO_4$ and ethanol (1:4, v/v) at a constant voltage of 20 V for 5 min below 278 K. Then, the specimen was anodized in 0.1 mol dm^{-3} ammonium pentaborate ($(NH_4)_2B_{10}O_{16}$) at a constant current density of 5 mA cm^{-2} up to 200 V at 293 K, using a two-electrode cell

with a platinum counter electrode. The alumina surface thus prepared was smooth and flat, as reported previously [27].

2.2 Characterizations

The surface and cross-section of the specimens were observed by a JEOL JSM-6500F field emission scanning electron microscope (SEM) and a JEOL JEM-2000FX transmission electron microscope (TEM) with EDS facilities, respectively. The cross-sectional specimen was prepared by focused gallium ion beam processing with a JEOL JIB-4600F/HKD multibeam system. Surface roughness was also evaluated using a KEYENCE VK09700 laser microscope. Phases in the anodically deposited CeO_2 layer formed on the stainless steel surface were identified by X-ray diffraction using a Rigaku RINT-2000 diffractometer with Cu Kα radiation (λ = 0.15418 nm). An α-2θ scan mode with α = 1° was used in this study. Elemental depth profile analysis was carried out by glow discharge optical emission spectroscopy (GDOES) using a Jobin-Yvon 5000 RF instrument in an argon atmosphere of 700 Pa by applying a power of 30 W. Light emissions of characteristic wavelength were monitored throughout the analysis with a sampling time of 0.01 s to obtain depth profile. The wavelength of the spectral lines used were 413.717 nm for cerium, 130.217 nm for oxygen, 385.991 nm for iron, 425.433 nm for chromium, 341.477 nm for nickel and 165.701 nm for carbon. The signals were detected from a circular area of approximately 4 mm diameter. The X-ray photoelectron spectra of the anodically deposited CeO_2 and anodic alumina surfaces after air exposure for 1, 7 and 12 h in a laboratory atmosphere were measured

using a JEOL JPS-9200 spectroscope with Mg Kα excitation (hν = 1253.6 eV). Binding energies of the photoelectrons were calibrated with a contaminant carbon peak energy (285.0 eV).

2.3 Wettability evaluation.

Surface wettability was evaluated by static and dynamic contact angle measurements for water droplet (4 μL) on specimen surfaces by a Kyowa Interface Science DM-CE1 contact angle measurement system after air exposure for various periods of time in a laboratory atmosphere. Dynamic contact angle measurements were performed by an expansion and contraction method. Contact angle values used in this study were average data of five different points on each specimen.

For examination of the self-healing hydrophobicity, oxygen plasma was irradiated for 4 min using a Harrick Plasma PDC-32G air plasma cleaner to the hydrophobic CeO_2 surface specimen in order to decompose organic contaminants on the surface. Then, water contact angle (WCA) was monitored during subsequent air exposure. This process was repeated several times.

3. Results and discussion

3.1 CeO_2 coating on stainless steel plate

Figures 1a and 1b show SEM micrographs of the surface of the electropolished stainless steel plate after anodic deposition of CeO_2. The surface appears rather smooth at low magnification (Fig. 1a), while high magnification micrograph (Fig. 1b) discloses

that the coating consists of densely packed nanoparticles with 10-15 nm in diameter. In Fig. 1a, microcracks are also found in the coating, probably associated with the shrinkage of the coating, which is caused by dehydration of the anodically deposited coating during drying [28]. Kulp et al. deposited anodically CeO_2 at 0.5 and 1.1 V vs Ag/AgCl in Ce(III) acetate solution [29]. They obtained a smooth and crack-free film at 0.5 V vs Ag/AgCl, while a film formed at 1.1 V vs Ag/AgCl contained nanoparticles. They suggested that the nanoparticles were formed because of indirect oxidation of Ce(III) with O_2, which was generated by electrochemical oxidation of water. The presence of nanoparticles in the present coating suggests such indirect mechanism of the formation of CeO_2. In fact, we found gas generation on anode during anodic deposition.

TEM observation of the coating cross-section (Fig. 1c) reveals that the coating is approximately 60 nm thick and uniform in thickness. EDX analysis of the marked region in Fig. 1c indicated the atomic ratio of Ce:O close to 1:2, corresponding to the composition of CeO_2. Figure 2 shows the X-ray diffraction pattern and GDOES elemental depth profile of the anodically deposited CeO_2 on the electropolished stainless steel plate. Only a CeO_2 phase (JCPDS card 34-0394) is identified from the X-ray diffraction pattern, apart from the reflections from the stainless steel substrate (Fig. 2a). The species (Fe, Ni and Cr) derived from the stainless steel substrate are not detected within the coating in the GDOES elemental depth profile analysis (Fig. 2b). Thus, rather pure CeO_2 is deposited on the stainless steel, although, from the depth profile, hydrogen and carbon impurity species appear to be slightly incorporated in the coating. The

incorporated carbon species may be derived from hexamethylenetetramine added in the coating solution.

Then, the wettability of the CeO_2-coated specimen was examined by static contact angle measurements. Figure 3 shows the WCAs and optical photographs of water droplets on the surfaces of the CeO_2 coating on electropolished stainless steel and the flat alumina film formed by anodizing of aluminum as a function of air exposure time. The WCA of the CeO_2 coating on the flat stainless steel is only 20^o immediately after deposition; the anodically deposited CeO_2 is hydrophilic. This is contrast to the hydrophobicity of the magnetron-sputtered CeO_2 surface [20]. However, the WCA gradually increases with time of air exposure and reaches ~104^o after three days. This means that the CeO_2 surface changes from hydrophilic to hydrophobic during air exposure. On the other hand, the WCA on the alumina surface remained hydrophilic even after three days.

In order to examine the change in composition of the CeO_2 and Al_2O_3 surface during air exposure, XPS surface analysis was performed. Figures 4a-c show the Ce 3d, O 1s and C 1s photoelectron spectra of the CeO_2 surface. The Ce 3d spectra in Fig. 4a are composed of two multiplets (i.e., v and u), which correspond to the spin orbit split $3d_{5/2}$ and $3d_{3/2}$, respectively. In accord with previous reports [30-34], the v, v'', v''', u, u'' and u''' peaks are attributed to Ce^{4+} state, while the v' and u' peaks are assigned to Ce^{3+} state. The intensity of all the Ce 3d peaks slightly decreases with time of air exposure. This is because of covering coating surface by hydrocarbon contaminants, as described below.

The O 1s spectra reveal two peaks at 529.5 eV and 531.4 eV; the former is assigned to Ce-O-Ce and the latter to $-OH/H_2O$ oxygen, defective oxide or carbonate oxygen [30, 35, 36]. The presence of surface $-OH/H_2O$ species probably make the surface hydrophilic. During air exposure, the intensity of $-OH/H_2O$ peak decreases slightly. The most significant change in the spectra was found in C 1s spectra during air exposure. The contaminant hydrocarbon peak at 285.0 eV becomes intense largely during air exposure, indicating the accumulation of hydrocarbon layer on the CeO_2 surface. A small peak at 289.0 eV is assigned to carboxyl or carbonate species [37, 38], whose intensity remains almost unchanged during air exposure.

The change in the XPS spectra of the Al_2O_3 surface during air exposure was also examined (Figs. 4d-f). The Al 2p spectra shows a peak at 74.3 eV, corresponding to Al^{3+} state [39]. A broad O 1s peak is owing to overlapping of Al-O-Al (530.9 eV) and OH/H_2O (531.8 eV) peaks. The intensity of the C 1s hydrocarbon peak (285.0 eV) increases with air exposure, but the increase in the intensity for Al_2O_3 surface is much less than that on the CeO_2 surface. As a consequence, only CeO_2 surface changes from hydrophilic to hydrophobic during air exposure.

Preston et al. reported the hydrophobicity of a CeO_2 pellet after air exposure for long time, similar to this study [23]. According to their report, a hydrophilic CeO_2 pellet surface conversed to hydrophobic due to adsorption of hydrocarbon contaminants compared to silica or gold surfaces; the WCA reaches 90^o after air exposure for 96 h. In addition, this trend has been shown for a variety of non-noble metal oxide materials including zirconia and titania, and occurs due to physisorption of hydrocarbons to –OH

groups and other energetically favorable sites present on the surface, where physical or chemical interactions are possible. In other words, hydrocarbon in the atmosphere can be adsorbed on the surface with high density of –OH groups [23, 40]. Thus, it is likely that the difference of wettability behavior between CeO_2-coated stainless steel and flat anodized alumina is owing to the difference of the amount of –OH groups on the surfaces. The anodically deposited CeO_2 surface may contain a high density of surface –OH group, promoting the accumulation of hydrocarbon contaminants from air. As a consequence, the surface becomes hydrophilic in air exposure. In fact, the deconvolution of O 1s spectra showed that approximately 40% of oxygen was –OH/H_2O-type on the as-deposited CeO_2 and that on the as-formed Al_2O_3 was only ~10%.

3.2 Introduction of surface roughness of CeO_2 for superhydrophobicity

Since the WCA as high as ~104^o is obtained by anodic deposition of CeO_2 on the flat stainless steel surface, we tried to introduce surface roughness to make the surface superhydrophobic. The rough surface was developed in this study by electrochemical etching of stainless steel prior to CeO_2 deposition. Figure 5 shows SEM micrographs of the electrochemically etched stainless steel surface before and after CeO_2 deposition. Numbers of semi-spherical large etch pits with several sizes of 50-100 μm (Fig. 5a), ~5 μm and 0.1-0.5 μm (Fig. 5b) are formed by the etching. Such surface morphology was remained even after deposition of CeO_2, and from the comparison of the high magnification images obtained before and after deposition (Figs 5c and 5f), 10 nm scale

roughness is further introduced after the deposition because of the formation of nano-particular CeO_2.

Figure 6 shows the change in WCA on CeO_2-coated flat and etched stainless steel surface with air exposure time. Immediately after deposition, the CeO_2 surface on the etched stainless steel is again hydrophilic, and the WCA is as low as 13^o, which is lower than that on flat stainless steel (20^o). The lower WCA on the etched specimen is explained from the Wenzel equation [41]:

$$\cos\theta_R = R\cos\theta_F \quad (1)$$

in which θ_R and θ_F are the WCAs on rough and flat surfaces and R is the roughness factor (R >1). This equation indicates that θ_R decreases with surface roughening when the θ_F is less than 90^o. Thus, the reduced WCA of the CeO_2 coating on the etched stainless steel in comparison with that on the flat stainless steel is qualitatively explained by surface roughening. After air exposure for 3 days, the WCA reaches 130^o on the etched specimen, being higher than that on the flat specimen (104^o). The R value estimated from the equation 1 is 2.66. The roughness was also estimated using a laser microscope, which indicated the roughness factor of 2.57. These two values are close to each other, suggesting that the water droplet on the CeO_2 coating on the etched stainless steel is in the Wenzel state. The roughness is not high enough for superhydrophobicity.

On the superhydrophobic surface, on which a water droplet is readily rolling off, a Cassie-Baxter state must be achieved. In this case, air pockets are present between the water droplet and the rough solid surface. Because of the reduced liquid/solid contact area, the water is rolling off more readily in comparison with the Wenzel state,

in which all the rough solid surface is contacted with liquid. To obtain a superhydrophobic CeO_2 surface by further enhancing the surface roughness, we utilized stainless steel mesh (mesh opening of 15 μm and wire diameter also of 15 μm) as substrate. Figure 7 shows scanning electron micrographs of the etched and non-etched stainless steel mesh with and without CeO_2 coating. The electrochemically etched mesh (Figs. 7a-c) discloses surface roughness and the grooves developed by the etching extends along with the wire direction (Fig. 7b). The roughness is remained even after CeO_2 deposition (Figs. 7d-f) and further nanoscale roughness is introduced by nanoparticle nature of CeO_2. High roughness of the etched mesh with CeO_2 is obvious from the comparison with the non-etched counterpart (Figs. 7g-i).

Fig. 8a shows the WCAs on the CeO_2-coatings on various stainless steel morphologies after air exposure for 3 days. The WCA on the CeO_2-coated stainless steel mesh without etching is only 121.3^o, which is lower than that on the etched stainless steel plate. The electrochemical etching of the stainless steel mesh increases the WCA remarkably and the WCA reaches 155.7^o. The dynamic WCA was also measured for the CeO_2 coated on the etched stainless steel mesh. The advancing and receding contact angles were 159.4^o and 157.4^o, respectively and the contact angle hysteresis is as low as 2.0° (Fig. 8b); the surface is superhydrophobic.

Figure 9 shows the schematic illustration showing the wetting behavior of the CeO_2 surface coated on etched stainless steel plate and mesh. The coating on the etched stainless steel plate was hydrophobic but not superhydrophobic. As discussed above, the surface is in the Wenzel state (Fig. 9a) [41]. Similarly, the CeO_2 coating on the stainless

steel mesh without electrochemical etching is hydrophobic from the WCA shown in Fig. 8a, but not superhydrophobic. Rather smooth wire surface of the mesh allows water to penetrate through the mesh.

On the other hand, it is most likely that the CeO_2 coating on the etched stainless steel mesh surface was in the Cassie-Baxter state due to superhydrophobicity, as shown in Fig. 9c. Assuming the Cassie-Baxter state, the *f* value in the equation (2) is estimated to be as low as 0.12 from the θ_R and θ_F values of 155.7 and 104.1, respectively [42].

$$\cos \theta_R = f (1 + \cos \theta_F) -1 \qquad (2)$$

This *f* value suggests that only a limited part of the mesh wires, roughly 4 μm width of the top part of the mesh wire, may be in contact with water droplet. Pinning of the water droplet by surface roughness of the mesh introduced by electrochemical etching is effective in achieving the superhydrophobic state.

3.4 Self-healing property of superhydrophobic CeO_2 surface

Since the superhydrophobic CeO_2 surface was obtained by accumulation of a carbon contaminant layer from the atmosphere, superhydrophobicity will be self-healed even after removing the hydrocarbon surface layer. In this study, we examined the self-healing behavior after oxygen plasma treatment of the superhydrophobic CeO_2 surface. As shown in Fig. 10, the high WCA of $>150^o$ changes to $\sim0^o$ after oxygen plasma treatment, probably because of the decomposition of the contaminant hydrocarbon layer and the introduction of surface −OH group by oxygen plasma [43, 44]. However, the WCA recovers again to $>150^o$ during air exposure for 72 h, and the

superhydrophilic to superhydrophobic transition due to re-accumulation of contaminant hydrocarbons occurs repeatedly as shown in this Figure. Findings demonstrate that the present CeO_2 coating possess the self-healing nature of superhydrophobicity.

Low durability is one of the critical issues for the practical use of superhydrophobic materials. Self-healing property is, therefore, of crucial importance to enhance the durability [45-49]. The present superhydrophobic CeO_2 surface on the stainless steel mesh showed the self-healing property because hydrophobic surface layer is derived from hydrocarbon in the atmosphere. In addition, rough CeO_2 surface is readily be prepared by a combination of simple electrochemical processes. The hierarchical CeO_2 surface formed by the electrochemical approach is, therefore, promising as a practical self-healing superhydrophobic material.

3.5 Application to oil/water separation

Since the etched stainless steel mesh with CeO_2 coating is superhydrophobic and superoleophilic as shown in Figs. 12a and b, we attempt to apply the CeO_2-coated stainless steel mesh for oil/water separation. When a mixture of oil (cyclohexane: surface tension, γ = 25.3 mN m^{-1}) and water (γ = 72.8 mN m^{-1}) was poured onto the etched stainless steel mesh coated with CeO_2, only cyclohexane penetrated through the mesh, but no penetration of water occurred, resulting in almost complete oil/water separation (Fig. 11c and Movie S1). Thus, we succeeded in separating an oil/water mixture by electrochemical etching and CeO_2 coating without low-surface-tension treatment by another coating such as organic self-assembled monolayers.

4. Conclusions

In summary, CeO_2 coating anodically deposited on a flat stainless steel surface is hydrophilic immediately after deposition, while converts to hydrophobic after exposure to the atmosphere. This wettability transition is due to accumulation of hydrocarbon contaminant in air. Superhydrophobic CeO_2 surface is obtained by the deposition of CeO_2 on the electrochemically etched stainless steel mesh with sufficiently high roughness after air exposure. The superhydrophobic CeO_2 surface also exhibits self-healing property. Self-healing property is of crucial importance for the improvement of low durability of superhydrophobic surfaces.

Acknowledgement

This work was supported in part by Adaptable & Seamless Technology Transfer Program through Target-driven Research and Development (A-STEP) from the Japan Science and Technology Agency, the “Nanotechnology platform” Program of the Ministry of Education, Culture, Sports, Science and Technology (MEXT), and JSPS KAKENHI Grant Number 15J00802.

References

[1] Y. Lu, S. Sathasivam, J. Song, C. R. Crick, C. J. Carmalt, I. P. Parkin, Repellent materials. Robust self-cleaning surfaces that function when exposed to either air to oil, Science 347 (2015) 1132-1135.

[2] F. Zhang, L. Zhao, H. Chen, S. Xu, D. G. Evans, X. Duan, Corrosion resistance of superhydrophobic layered double hydroxide films on aluminum, Angew. Chem. Int. Ed. 47 (2008) 2466-2469.

[3] R. Jafari, R. Menini, M. Farzaneh, Superhydrophobic and icephobic surfaces prepared by RF-sputtered polytetrafluoroethylene coatings, Appl. Surf. Sci. 257 (2010) 1540-1543.

[4] H. Zhang, R. lamb, J. Lewis, Engineering nanoscale roughness on hydrophobic surface-preliminary assessment of fouling behaviour, Sci. Technol. Adv. Mater. 6 (2005) 236-239.

[5] Y. Cheng, D. E. Rodak, Is the lotus leaf superhydrophobic?, Appl. Phys. Lett. 86, (2005) 144101.

[6] V. Zorba, E. Stratakis, M. Barberouglou, E. Spanakis, P. Tzanetakis, S. H. Anastasiadis, C. Fotakis, Biomimetic Artificial surfaces quantitatively reproduce the water repellency of a lotus leaf, Adv. Mater. 20 (2008) 4049-4054.

[7] X. Gao, L. Jiang, Water-repellent legs of water striders, Nature 432 (2004) 36.

[8] S. Niu, B. Li, Z. Mu, M. Yang, J. Zhang, Z. Han, L. Ren, Excellent structure-based multifunction of morpho butterfly wings: A Review, J. Bionic Eng. 12 (2015) 170-189.

[9] T. Onda, S. Shibuichi, N. Satoh, K. Tsujii, Super-water-repellent fractal surfaces, Langmuir 12, (1996) 2125-2127.

[10] K. Tadanaga, N. katata, T. Minami, Formation process of super-water-repellent Al_2O_3 coating films with high transparency by the sol–gel method, J. Am. Ceram. Soc. 80 (1997) 3213-3216.

[11] L. Feng, S. Li, Y. Li, H. Li, L. Zhang, J. Zhai, Y. Song, B. Liu, L. Jiang, D. Zhu, Super-hydrophobic surfaces: from natural to artificial, Adv. Mater. 12 (2002) 1857-1860.

[12] K. K. S. Lau, J. Bico, K. B. K. Teo, M. Chhowalla, G. A. J. Amaratunga, W. I. Milne, G. H. McKinley, K. K. Gleason, Superhydrophobic carbon nanotube forests, Nano Lett. 3, (2003) 1701-1705.

[13] K. Koch, B. Bhushan, Y. C. Jung, W. Barthlott, Fabrication of artificial lotus leaves and significance of hierarchical structure for superhydrophobicity and low adhesion, Soft Matter. 5 (2009) 1386-1393.

[14] B. Bhushan, Y. C. Jung, Natural and biomimetic artificial surfaces for superhydrophobicity, self-cleaning, low adhesion, and drag reduction, Prog. Mater. Sci. 56 (2011) 1-108.

[15] T. Fujii, Y. Aoki, H. Habazaki, Superhydrophobic hierarchical surfaces fabricated by anodizing of oblique angle deposited Al–Nb alloy columnar films, Appl. Surf. Sci. 257 (2011) 8282-8288.

[16] S. Yang, H. Habazaki, T. Fujii, Y. Aoki, P. Skeldon, G. E. Thompson, Control of morphology and surface wettability of anodic niobium oxide microcones formed in hot phosphate–glycerol electrolytes, Electrochim. Acta 56 (2011) 7446-7453.

[17] U. Manna, D. M. Lynn, Patterning and impregnation of superhydrophobic surfaces using aqueous solutions, ACS Appl. Mater. Interfaces 5 (2013) 7731-7736.

[18] J. Li, R. Kang, X. Tang, H. She, Y. Yang, F. Zha, Superhydrophobic meshes that can repel hot water and strong corrosive liquids used for efficient gravity-driven oil/water separation, Nanoscale 8 (2016) 7638-7645.

[19] B. Zhang, H. Feng, F. Lin, Y. Wang, L. Wang, Y. Dong, W. Li, Superhydrophobic surface fabricated on iron substrate by black chromium electrodeposition and its corrosion resistance property, Appl. Surf. Sci. 378 (2016) 388-396.

[20] G. Azimi, R. Dhiman, H. Kwon, A. T. Paxson, K. K. Varanasi, Hydrophobicity of rare-earth oxide ceramics, Nat. Mater. 12 (2013) 315-320.

[21] I. Oh, K. Kim, Z. Lee, K. Y. Ko, C. Lee, S. J. Lee, J. M. Myung, C. Lansalot-Matras, W. Noh, C. Dussarrat, H. Kim, H. Lee, Hydrophobicity of rare earth oxides grown by atomic layer deposition, Chem. Mater. 27 (2015) 148-156.

[22] F. Pedraza, S. A. Mahadik, B. Bouchaud, Synthesis of ceria based superhydrophobic coating on Ni20Cr substrate via cathodic electrodeposition, Phys. Chem. Chem. Phys. 17 (2015) 31750-31757.

[23] D. J. Preston, N. Miljkovic, J. Sack, R. Enright, J. Queemey, E. N. Wang, Effect of hydrocarbon adsorption on the wettability of rare earth oxide ceramics, Appl. Phys. Lett. 105 (2014) 011601.

[24] S. Khan, G. Azimi, B. Yildiz, K. K. Varanasi, Role of surface oxygen-to-metal ratio on the wettability of rare-earth oxides, Appl. Phys. Lett. 106 (2015) 061601.

[25] J. Tam, G. Palumbo, U. Erb, Recent advances in superhydrophobic electrodeposits, Materials 9 (2016) 1-27.

[26] C. Lee, A. Kim, J. Kim, Electrochemically etched porous stainless steel for enhanced oil retention, Surf. Coat. Technol. 264 (2015) 127-131.

[27] K. Shimizu, H. Habazaki, P. Skeldon, G.E. Thompson, R.K. Marcus, Radio frequency glow discharge optical emission spectroscopy: Depth profiling analysis of thin anodic alumina films as potential reference materials, Spectroscopy, 17 (2002) 14-18, 20, 22-23.

[28] L. Arurault, P. Monsang, J. Salley, R. S. Bes, Electrochemical preparation of adherent ceria coatings o ferritic stainless steel, Thin Solid Films 466 (2004) 75-80.

[29] E. A. Kulp, S. J. Limmer, E. W. Bohanman, J. A. Switzer, Solid State Ionics 178 (2007) 749–757.

[30] J. Xu, S. S. Xin, P. H. Han, R. Y. Ma, M. C. Li, Cerium chemical conversion coatings for corrosion protection of stainless steels in hot seawater environments, Mater. Corros. 64 (2013) 619-624.

[31] H. Ardelean, I. Frateur, P. Marcus, Corrosion protection of magnesium alloys by cerium, zirconium and niobium-based conversion coatings, Corros. Sci. 50 (2008) 1907-1918.

[32] S. Yang, W. Zhu, Z. Jiang, Z. Chen, J. Wang, The surface properties and the activities in catalytic wet air oxidation over CeO_2-TiO_2 catalysts, Appl. Surf. Sci. 252 (2006) 8499-8505.

[33] X. Gao, Y. Jiang, Y. Zhong, Z. Y. Luo, K. F. Cen, The activity and characterization of CeO_2-TiO_2 catalysts prepared by the sol-gel method for selective catalytic reduction of NO with NH_3, J. Hazard Mater. 174, (2010) 734-739.

[34] A. Q. Wang, P. Punchaipetch, R. M. Wallace, T. D. Goldenb, X-ray photoelectron spectroscopy study of electrodeposited nanostructured CeO_2, films, J. Vac. Sci. Technol. B 21 (2003) 1169-1175.

[35] M. Kang, E. D. Park, J. M. Kim, J. E. Yie, Manganese oxide catalysts for NO_x reduction with NH_3 at low temperatures, Appl. Catal. A 327 (2007) 261-269.

[36] L. Martinez, E. Roman, J. L. de Segovia, S. Poupard, J. Creus, F. Pedraza, Surface study of cerium oxide based coatings obtained by cathodic electrodeposition on zinc, Appl. Surf. Sci. 257 (2011) 6202-6207.

[37] W. Tseng, C. Tseng, C. Kuo, Effects of gas composition on highly efficient surface modification of multi-walled carbon nanotubes by cation treatment, Nanoscale Res Lett. 4 (2009) 234-239.

[38] D. Zhang, Y. Ma, H. Feng, Y. Hao, Adsorption of Cr(VI) from aqueous solution using carbon-microsilica composite adsorbent, J. Chil. Chem. Soc. 57 (2012) 964-968.

[39] T. Sugama, N. Carciello, Pyrogenic polygermanosiloxane coatings for aluminum substrates, J. Non-Cryst. Solids, 134 (1991) 58-70.

[40] S. Takeda, M. Fukawa, Y. Hayashi, K. Matsumoto, Surface OH group governing adsorption properties of metal oxide films, Thin Solid Films, 339 (1999) 220-224.

[41] R. N. Wenzel, Resistance of solid surfaces to wetting by water, Ind. Eng. Chem. 28 (1936) 988-994.

[42] A. B. D. Cassie, S. Baxter, Wettability of porous surfaces, Trans. Faraday Soc. 40 (1944) 546-551.

[43] A. L. Sumner, E. J. Menke, Y. Dubowski, J. T. Newberg, R. M. Penner, J. C. Hemminger, L. M. Wingen, T. Brauers, B. J. Finlayson-Pitts, The nature of water on surfaces of laboratory systems and implications for heterogeneous chemistry in the troposphere, Phys. Chem. Chem. Phys. 6 (2004) 604-613.

[44] S. B. Habib, E. Gonzalez II, R. F. Hicks, Atmospheric oxygen plasma activation of silicon (100) surfaces, Appl. Vac. Sci. Technol. A 28 (2010) 476-485.

[45] Y. Li, L. Li, J. Sun, Bioinspired self-healing superhydrophobic coatings, Angew. Chem. 122 (2010) 6265-6269.

[46] X. Wang, X. Lu, F. Zhou, W. Liu, Self-healing superamphiphobicity, Chem. Commun. 47 (2011) 2324-2326.

[47] C. Xue, Z. Zhang, J. Zhang, S. Jia, Lasting and self-healing superhydrophobic surfaces by coating of polystyrene/SiO_2 nanoparticles and polydimethylsiloxane, J. Mater. Chem. A 2 (2014) 15001-15007.

[48] D. Zhu, X. Lu, Q. Lu, Electrically conductive PEDOT coating with self-healing superhydrophobicity, Langmuir 30 (2014) 4671-4677.

[49] M. Wu, B. Ma, T. Pan, S. Chen, J. Sun, Silver-nanoparticle-colored cotton fabrics with tunable colors and durable antibacterial and self-healing superhydrophobic properties, Adv. Funct. Mater. 26 (2016) 569-576.

Figure cations

Fig. 1 Surface SEM images with (a) low and (b) high magnification and (c) a cross-sectional TEM image of Type 304 stainless steel plate after anodic deposition in solution containing 0.01 mol dm^{-3} $Ce(NO_3)_3$ and 0.05 mol dm^{-3} hexamethylenetetramine at a constant current density of 10 A m^{-2} for 60 min at 333 K.

Fig. 2 (a) XRD pattern and (b) GDOES elemental depth profile of the anodically deposited coating on Type 304 stainless steel plate in solution containing 0.01 mol dm^{-3} $Ce(NO_3)_3$ and 0.05 mol dm^{-3} hexamethylenetetramine at a constant current density of 10 A m^{-2} for 60 min at 333 K.

Fig. 3 (a) The WCAs as a function of exposure time in atmosphere and (b) optical images of water droplets on Type 304 stainless steel plate surface with CeO_2 coating and aluminum plate surface anodized in 0.1 mol dm^{-3} ammonium pentaborate aqueous solution up to 200 V at 293 K.

Fig. 4 XPS spectra of (a) Ce 3d, (b, e) O 1s, (c, f) C 1s and (d) Al 2p photoelectrons for (a-c) the CeO_2 coating surface anodically deposited on Type 304 stainless steel plate and (b-f) anodized aluminum surface after exposure for 0, 7 and 12 h in air.

Fig. 5 SEM surface images Type 304 stainless steel plate surface electrochemically etched in solution containing 1.2 wt.% HNO_3 and 3.6 wt.% HCl at a constant current density of 10 kA m^{-2} up to 4×10^6 C m^{-2} at 313 K (a-c) before and (d-f) after anodic deposition of CeO_2 in solution containing 0.01 mol dm^{-3} $Ce(NO_3)_3$ and 0.05 mol dm^{-3} hexamethylenetetramine at a constant current density of 10 A m^{-2} for 60 min at 333 K.

Fig. 6 The WCAs on stainless steel plate with or without electrochemical etching after anodic deposition of CeO_2 as a function of exposure time in air.

Fig. 7 SEM images of Type 304 stainless steel mesh surfaces electrochemically etched in solution containing 1.2 wt.% HNO_3 and 3.6 wt.% HCl at a constant current density of 100 A m^{-2} for 60 s at 313 K (a-c) before and (d-f) after anodic deposition of CeO_2 in

solution containing 0.01 mol dm^{-3} $Ce(NO_3)_3$ and 0.05 mol dm^{-3} hexamethylenetetramine at a constant current density of 10 A m^{-2} for 60 min at 333 K. The CeO_2 deposited on the non-etched stainless steel mesh are shown in (g-i).

Fig. 8 (a) The static WCAs on CeO_2 surface anodically deposited on Type 304 stainless steel plate and mesh surfaces with or without electrochemical etching after air exposure for 3 days and (b) optical images of the water droplets during dynamic contact angle measurements for the etched stainless steel mesh with CeO_2 coating.

Fig. 9 Schematic illustrations showing wetting of the CeO_2 anodically deposited on stainless steel: (a) the electrochemically etched stainless steel plate and (b) non-etched and (c) etched stainless steel mesh.

Fig. 10 The advancing and receding contact angles for water on the CeO_2 coating anodically deposited on the electrochemically etched Type 304 stainless steel mesh after several consecutive oxygen plasma treatment for 2 min and exposure in air for 72 h.

Fig. 11 Optical images of (a) water and cyclohexane droplets on the superhydrophobic CeO_2 coating on the electrochemically etched Type 304 stainless steel mesh and (b) the oil/water separation test.

Supplementary materials

Movie S1 Separation of a mixture of water and cyclohexane (1:1, v/v) using a superhydrophobic CeO_2 coating on the electrochemically etched Type 304 stainless steel mesh.

1 Graphical abstract

2

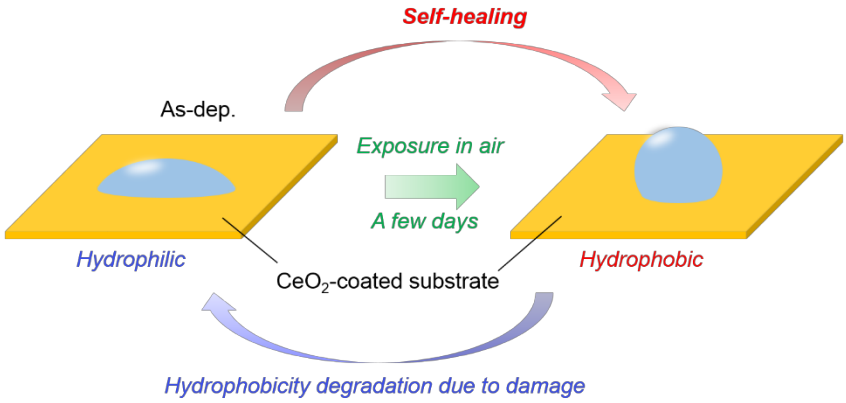

3

4

5

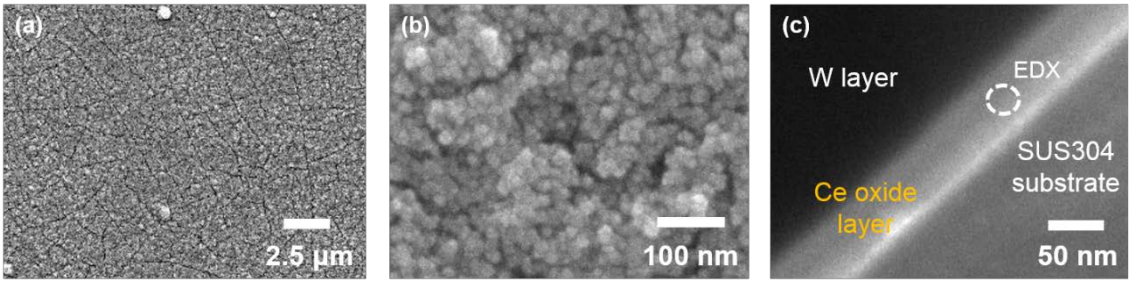

Fig. 1 Surface SEM images with (a) low and (b) high magnification and (c) a cross-sectional TEM image of Type 304 stainless steel plate after anodic deposition in solution containing 0.01 mol dm^{-3} $Ce(NO_3)_3$ and 0.05 mol dm^{-3} hexamethylenetetramine at a constant current density of 10 A m^{-2} for 60 min at 333 K.

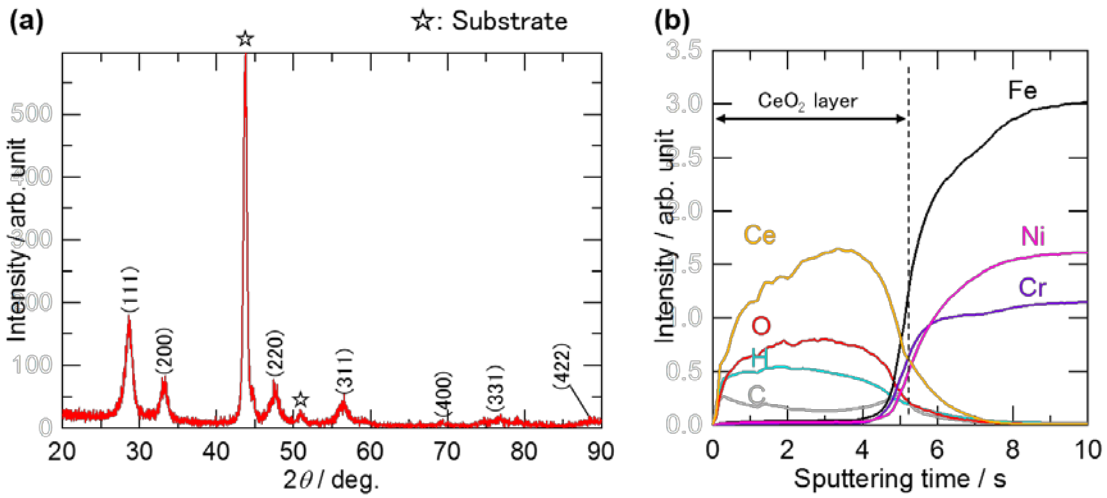

Fig. 2 (a) XRD pattern and (b) GDOES elemental depth profile of the anodically deposited coating on Type 304 stainless steel plate in solution containing 0.01 mol dm^{-3} $Ce(NO_3)_3$ and 0.05 mol dm^{-3} hexamethylenetetramine at a constant current density of 10 A m^{-2} for 60 min at 333 K.

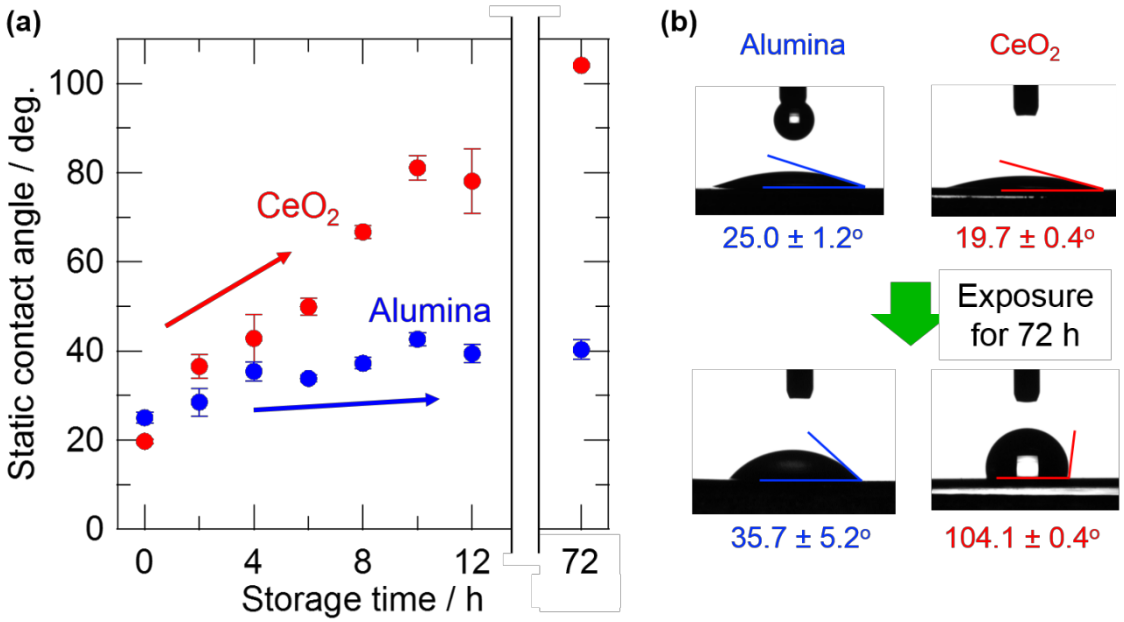

Fig. 3 (a) The WCAs as a function of exposure time in atmosphere and (b) optical images of water droplets on Type 304 stainless steel plate surface with CeO_2 coating and aluminum plate surface anodized in 0.1 mol dm^{-3} ammonium pentaborate aqueous solution up to 200 V at 293 K.

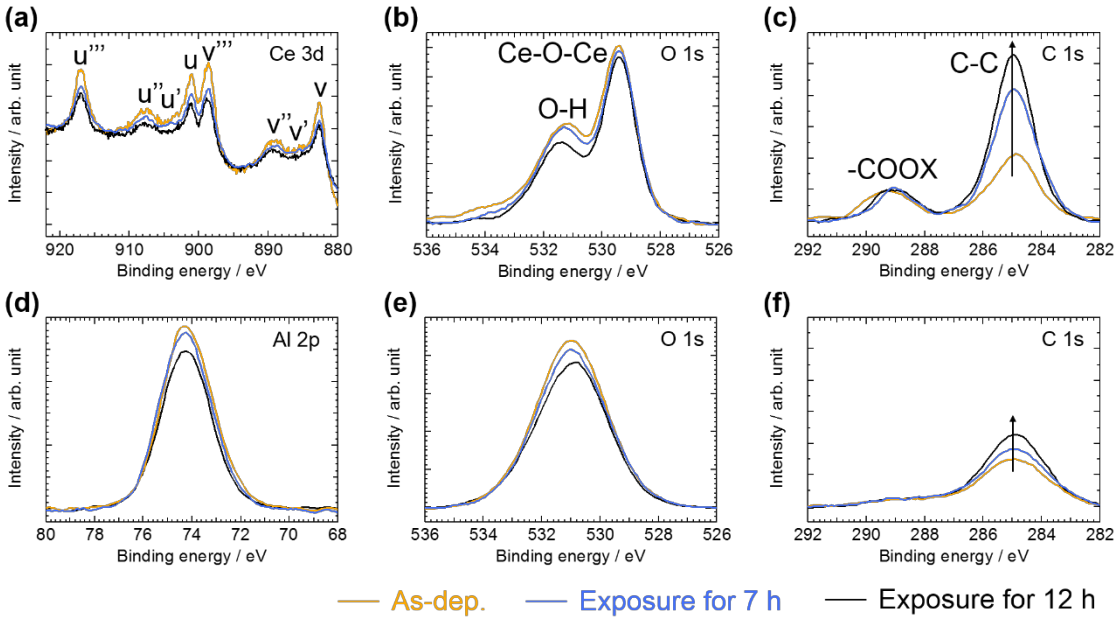

Fig. 4 XPS spectra of (a) Ce 3d, (b, e) O 1s, (c, f) C 1s and (d) Al 2p photoelectrons for (a-c) the CeO_2 coating surface anodically deposited on Type 304 stainless steel plate and (b-f) anodized aluminum surface after exposure for 0, 7 and 12 h in air.

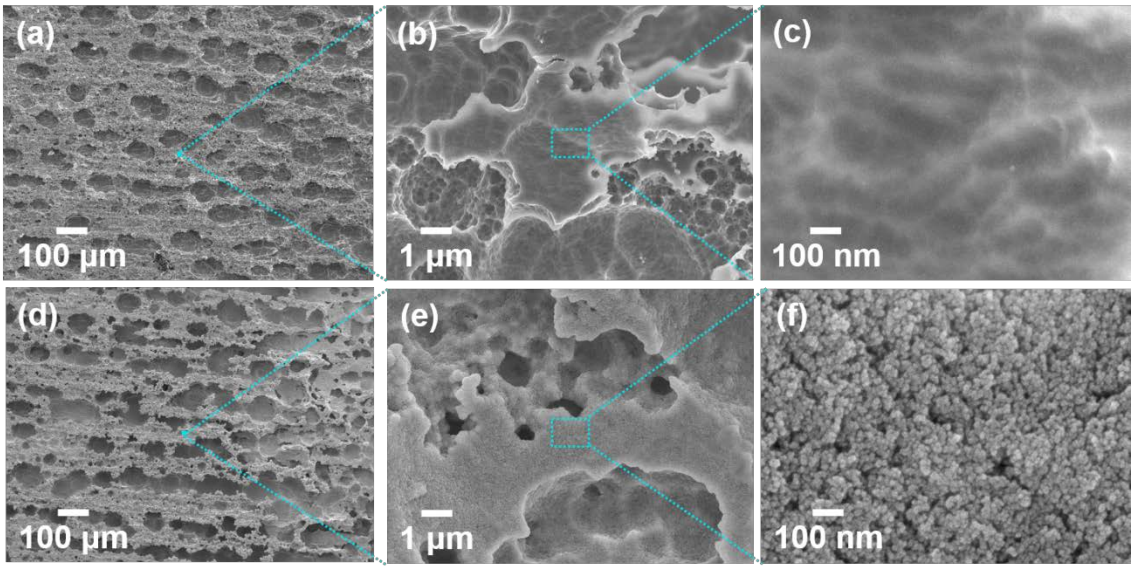

Fig. 5 SEM surface images Type 304 stainless steel plate surface electrochemically etched in solution containing 1.2 wt.% HNO_3 and 3.6 wt.% HCl at a constant current density of 10 kA m^{-2} up to 4×10^6 C m^{-2} at 313 K (a-c) before and (d-f) after anodic deposition of CeO_2 in solution containing 0.01 mol dm^{-3} $Ce(NO_3)_3$ and 0.05 mol dm^{-3} hexamethylenetetramine at a constant current density of 10 A m^{-2} for 60 min at 333 K.

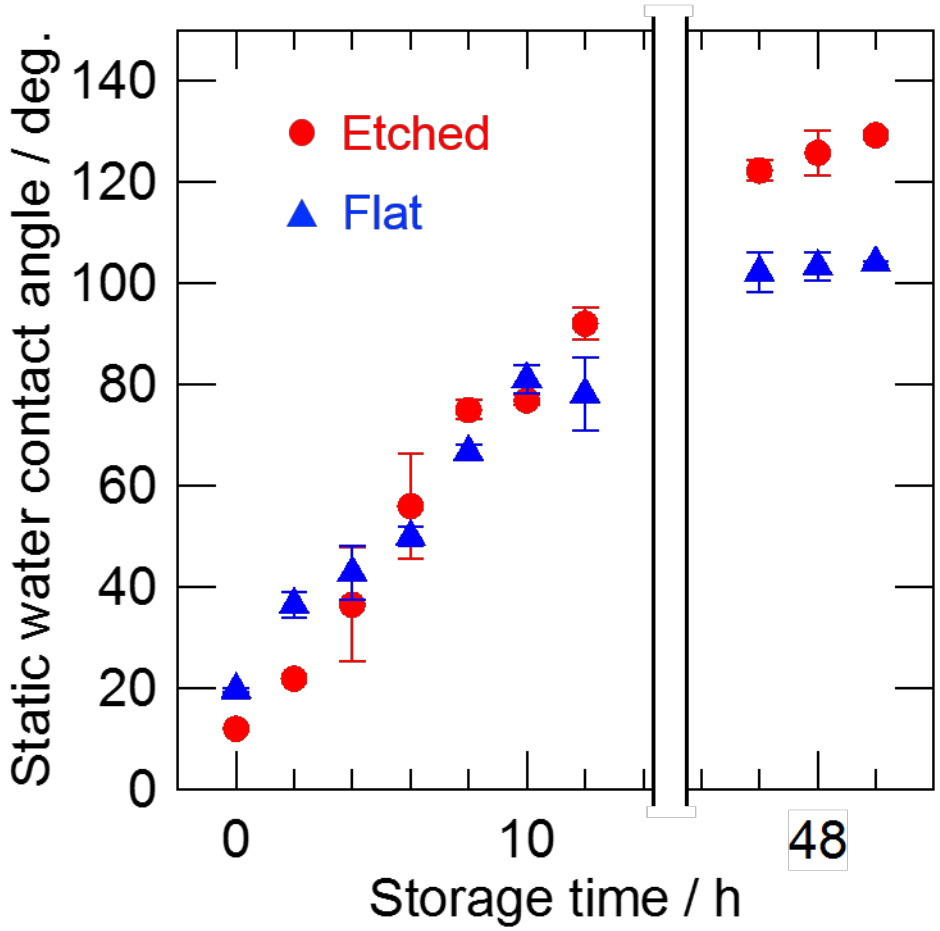

Fig. 6 The WCAs on stainless steel plate with or without electrochemical etching after anodic deposition of CeO_2 as a function of exposure time in air.

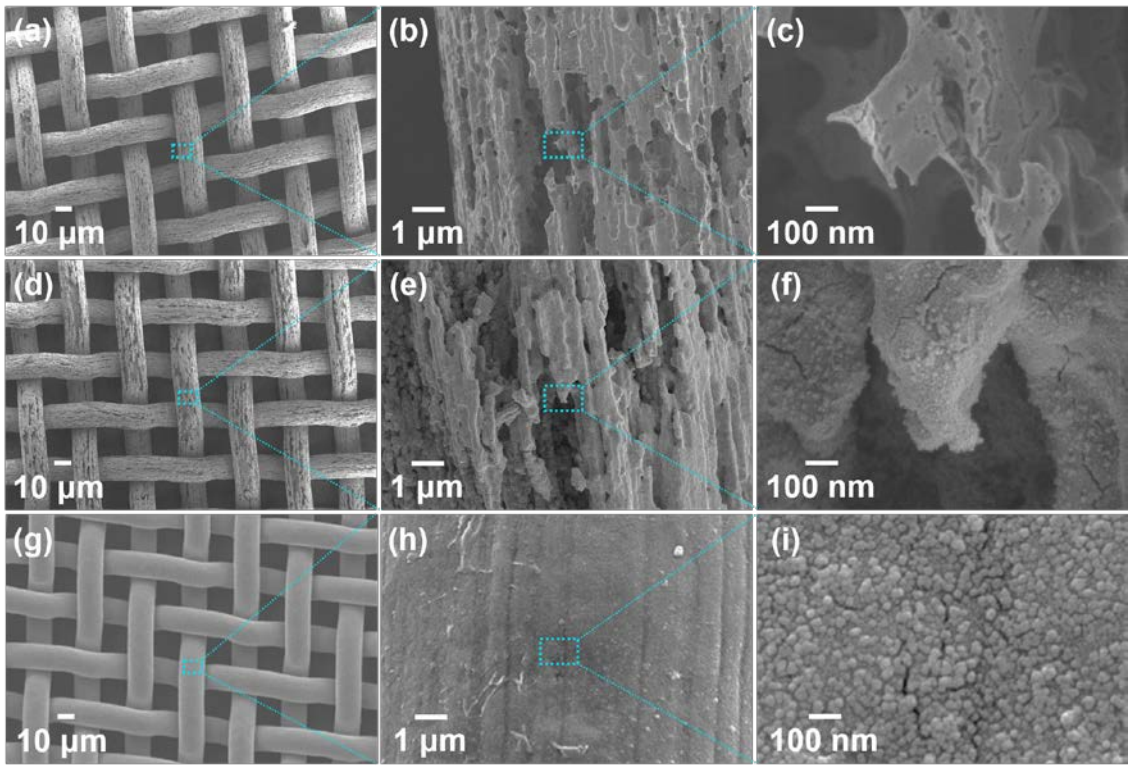

Fig. 7 SEM images of Type 304 stainless steel mesh surfaces electrochemically etched in solution containing 1.2 wt.% HNO_3 and 3.6 wt.% HCl at a constant current density of 100 A m^{-2} for 60 s at 313 K (a-c) before and (d-f) after anodic deposition of CeO_2 in solution containing 0.01 mol dm^{-3} $Ce(NO_3)_3$ and 0.05 mol dm^{-3} hexamethylenetetramine at a constant current density of 10 A m^{-2} for 60 min at 333 K. The CeO_2 deposited on the non-etched stainless steel mesh are shown in (g-i).

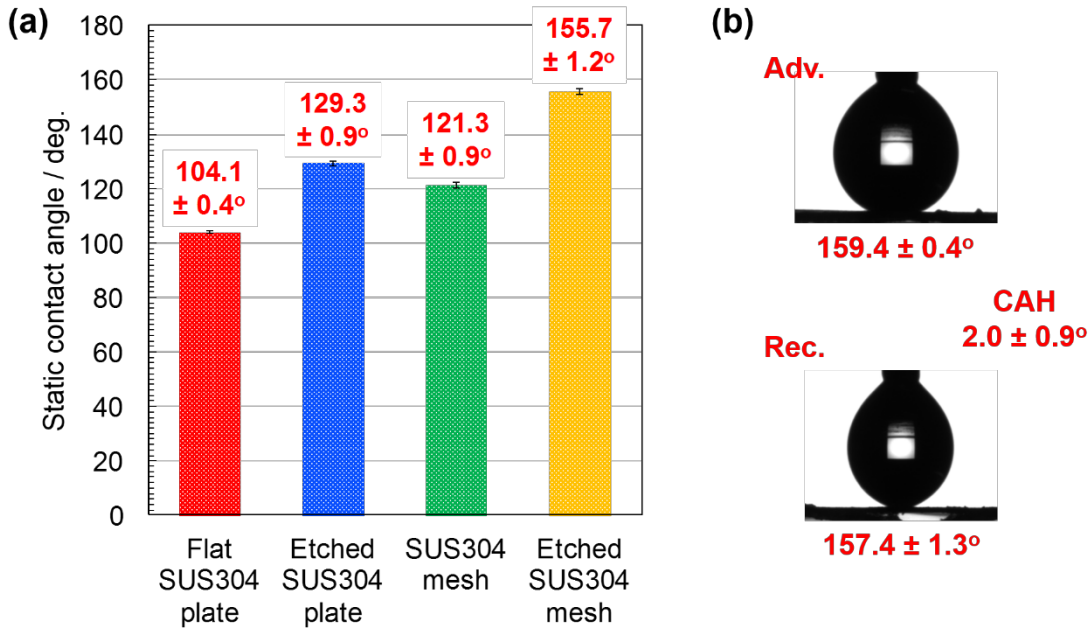

Fig. 8 (a) The static WCAs on CeO_2 surface anodically deposited on Type 304 stainless steel plate and mesh surfaces with or without electrochemical etching after air exposure for 3 days and (b) optical images of the water droplets during dynamic contact angle measurements for the etched stainless steel mesh with CeO_2 coating.

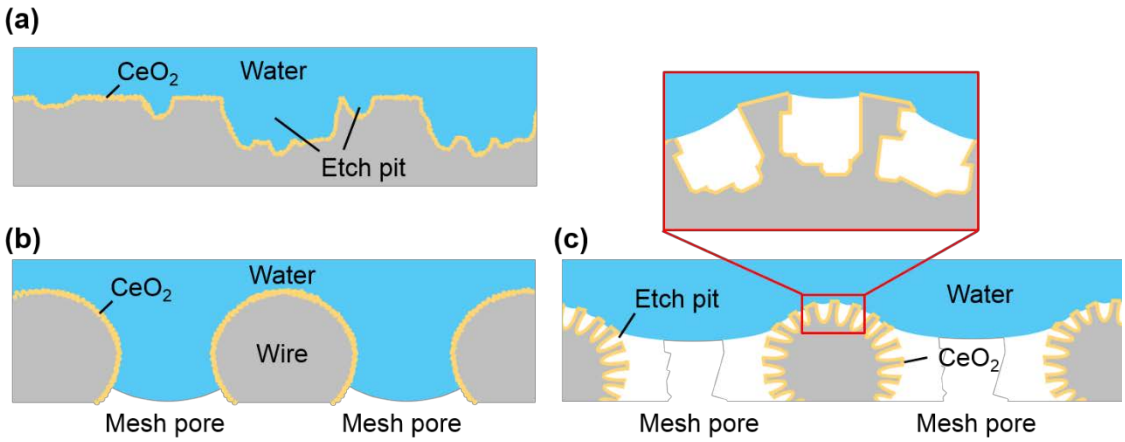

Fig. 9 Schematic illustrations showing wetting of the CeO_2 anodically deposited on stainless steel: (a) the electrochemically etched stainless steel plate and (b) non-etched and (c) etched stainless steel mesh.

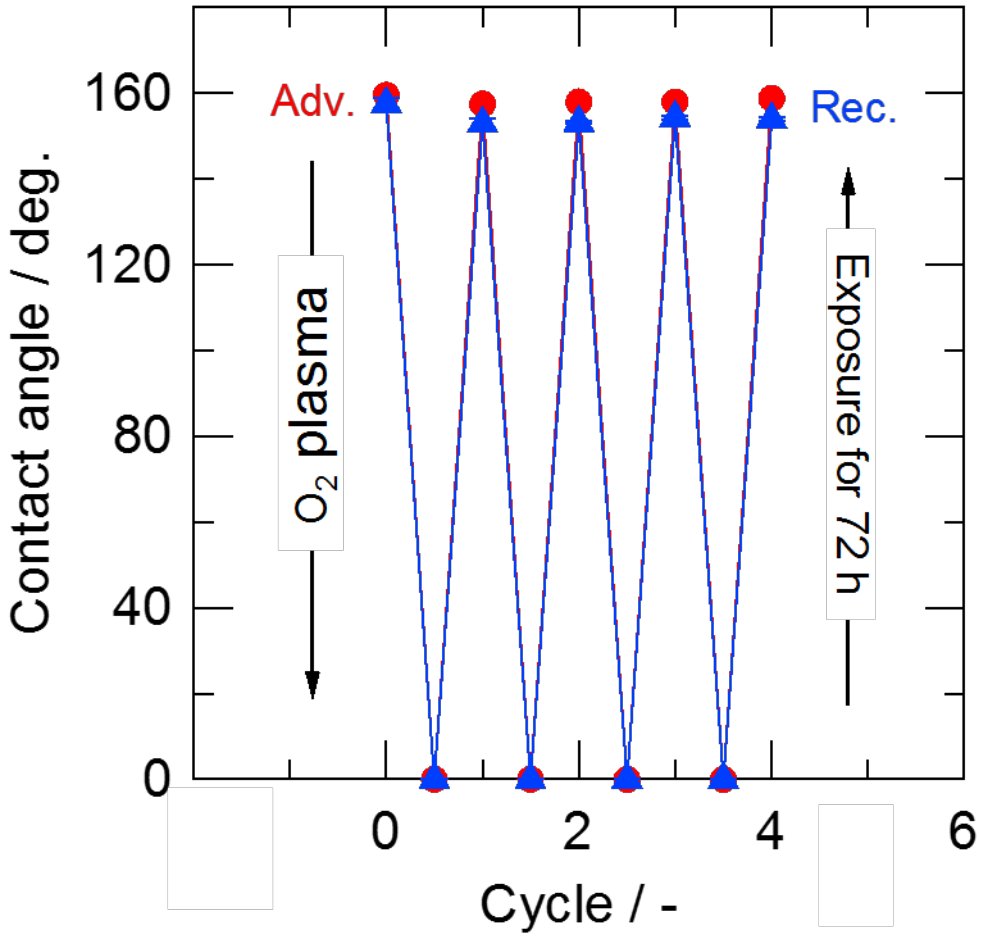

Fig. 10 The advancing and receding contact angles for water on the CeO_2 coating anodically deposited on the electrochemically etched Type 304 stainless steel mesh after several consecutive oxygen plasma treatment for 2 min and exposure in air for 72 h.

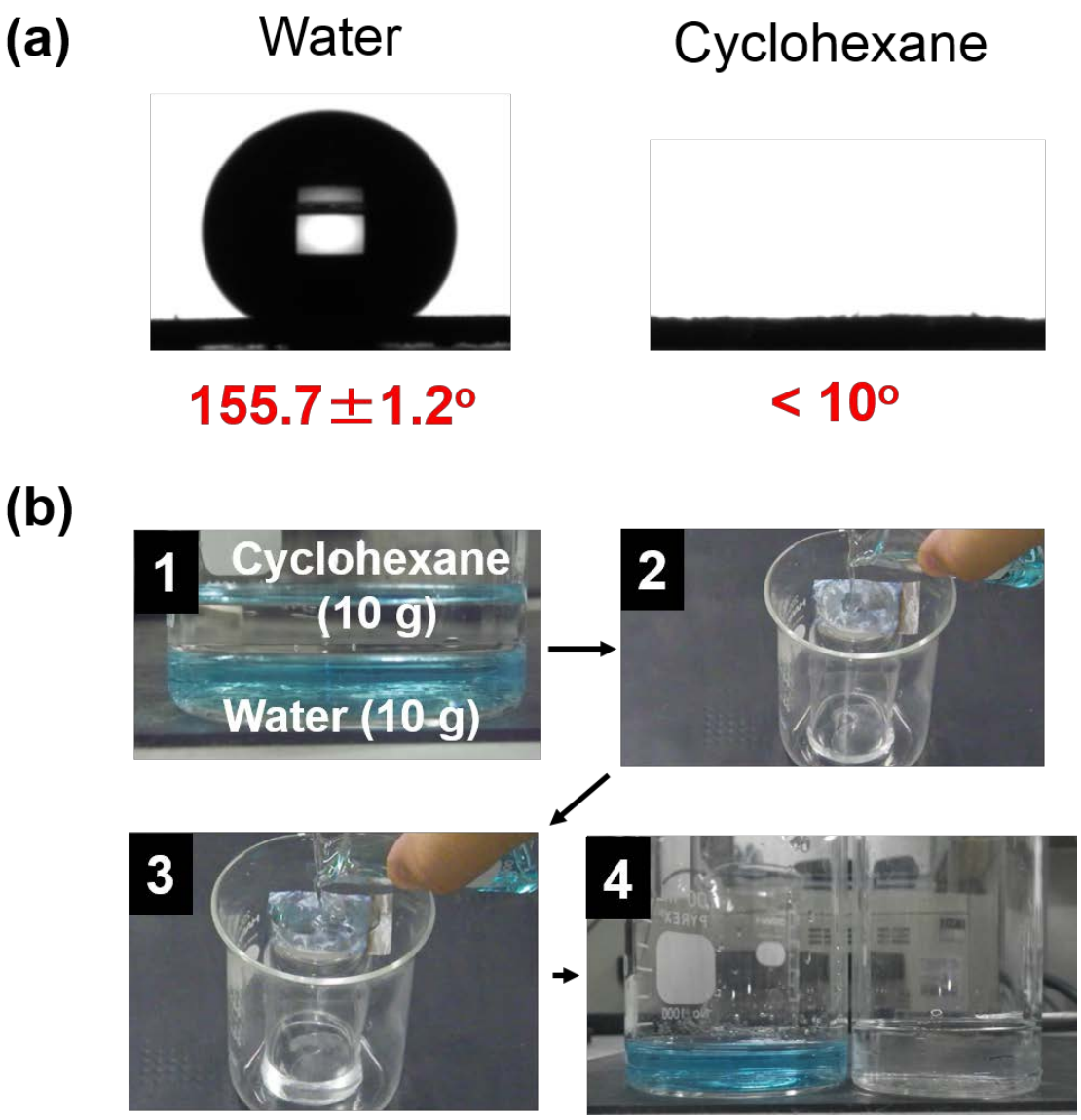

Fig. 11 Optical images of (a) water and cyclohexane droplets on the superhydrophobic CeO_2 coating on the electrochemically etched Type 304 stainless steel mesh and (b) the oil/water separation test.